JOURNAL OF Applied Polymer SCIENCE

Preparation and Properties of TiO_2-Filled Poly(acrylonitrile-butadiene-styrene)/Epoxy Hybrid Composites

Jyotishkumar P,[1] Jürgen Pionteck,[2] Paula Moldenaers,[3] Sabu Thomas[1,4,5,6]

[1]School of Chemical Sciences, Mahatma Gandhi University, Priyadarshini Hills, Kottayam 686560, Kerala, India
[2]Department of Polymer Reactions and Blends, Leibniz-Institute for Polymer Research Dresden, 01069 Dresden, Germany
[3]Department of Chemical Engineering, Catholic University of Leuven, B-3001, Leuven, Belgium
[4]Centre for Nanoscience and Nanotechnology, Mahatma Gandhi University, Priyadarshini Hills, Kottayam 686560, Kerala, India
[5]Universiti Teknologi MARA, Faculty of Applied Sciences, 40450 Shah Alam, Selongor, Malaysia
[6]Center of Excellence for Polymer Materials and Technologies, Tehnoloski Park 24, 1000 Ljubljana, Slovenia
Correspondence to: S. Thomas (E-mail: sabupolymer@yahoo.com)

ABSTRACT: Poly (acrylonitrile-butadiene-styrene) (ABS) was used to modify diglycidyl ether of bisphenol-A type of epoxy resin, and the modified epoxy resin was used as the matrix for making TiO_2 reinforced nanocomposites and were cured with diaminodiphenyl sulfone for superior mechanical and thermal properties. The hybrid nanocomposites were characterized by using thermogravimetric analyzer (TGA), dynamic mechanical analyzer (DMA), universal testing machine (UTM), scanning electron microscopy (SEM), and transmission electron microscopy (TEM). The bulk morphology was carefully analyzed by SEM and TEM and was supported by other techniques. DMA studies revealed that the DDS-cured epoxy/ABS/TiO_2 hybrid composites systems have two T_gs corresponding to epoxy and ABS rich phases and have better load bearing capacity with the addition of TiO_2 particles. The addition of TiO_2 induces a significant increase in tensile properties, impact strength, and fracture toughness with respect to neat blend matrix. Tensile toughness reveals a twofold increase with the addition of 0.7 wt % TiO_2 filler in the blend matrix with respect to neat blend. SEM micrographs of fractured surfaces establish a synergetic effect of both ABS and TiO_2 components in the epoxy matrix. The phenomenon such us cavitation, crack path deflection, crack pinning, ductile tearing of the thermoplastic, and local plastic deformation of the matrix with some minor agglomerates of TiO_2 are observed. However, between these agglomerates, the particles are separated well and are distributed homogeneously within the polymer matrix. © 2012 Wiley Periodicals, Inc. J. Appl. Polym. Sci. 000: 000–000, 2012

KEYWORDS: epoxy hybrid composites; thermo-mechanical properties; thermal stability; glass transition; fracture morphology

Received 14 July 2011; accepted 15 March 2012; published online
DOI: 10.1002/app.37729

INTRODUCTION

With the advance of science and technology, high-molecular weight materials become one of most attractive resources for advanced applications. Among them, epoxy resin is the most important in industry owing to its light weight, higher density, viscosity, excellent thermal stability, and cost effectiveness. However, its application range is limited because of its brittleness.[1] Among the existing modified processes, rubber-toughened epoxy resins lead to degraded strength and rigidity of materials and hence no significance in fiber composite applications.[2] An alternative approach to toughen epoxy polymers for fibre composite applications is the use of epoxy blend as matrix with high performance thermoplastics.[3–12] Recently, mixing nanosized materials into the epoxy resin has been proved as an ideal modification method to improve the mechanical and thermal properties of epoxy system owing to the large surface area of nanomaterials.[13–17] This helps to provide more opportunities for physical or chemical bonding with epoxy resin, thereby enhancing the interfacial bonding of particles and substrate. However, the unique nanocomposite effect can only be effective, if the nanoparticles are well dispersed in the surrounding polymer matrix. It is also reported that a considerable amount of improvement in mechanical properties can be achieved using very low amount of nanoparticles loadings.[18,19]

Nanoscaled TiO_2 embedded has gained great interests in the last decades because of unique properties and good performance. TiO_2 is extensively used in the industries such as additives of

epoxies, plastic, and rubber.[20–24] Recently, researches were inspired with the new concept "hybrid composites" for improved toughness. For example, the simultaneous addition of glass sphere and CTBN in to epoxy resin,[25] addition of clay and rubber in epoxy resin,[26,27] addition of nanosilica and CTBN in epoxy resin,[28] addition of MWCNT and (acrylonitrile-butadiene-styrene) (ABS) in epoxy resin,[29] hydroxyl-terminated polyether ether ketone having pendant methyl group (PEEKMOH), microballoon–nanoclay epoxy amine system,[30] etc. According to the literature, a synergetic effect in toughness was observed (in most of the studies) in hybrid composites. Current research is directed toward the use of both ABS and TiO_2 in an epoxy-amine system to achieve enhanced toughness. The curing kinetics, volume shrinkage, thermal, and mechanical properties of epoxy/ABS blends have been discussed in detail in our earlier studies.[12,31–33] It has been proved that 3.6 wt % ABS/epoxy blend possesses superior mechanical and thermal properties compared with the other blends. The main objective of this study is to explore the effect of TiO_2 loading in 3.6 wt % ABS/epoxy blend matrix. The thermal, mechanical, and morphological properties of hybrid composites were investigated as a function of TiO_2 composition. The relationship between the morphology and the thermo-mechanical properties of hybrid composites has been established.

EXPERIMENTAL

Materials

The matrix material used in the experiments consists of diglycidyl ether of bisphenol-A (DGEBA) (Lapox L-12, Atul, India) and 4,4′-diamino diphenyl sulfone (DDS) (Lapox K-10, Atul). The toughener ABS (Poly lac PA-757K) was manufactured by Chi Mei Corporation, Taiwan. The used ABS is a commercially available thermoplastic polymer consisting of 70 wt % polystyrene (PS), 25 wt % acrylonitrile (AN), and 5 wt % agglomerated polybutadiene (PB). The molecular weight of the soluble part of ABS was determined to be M_n = 51300 g/mol and M_w = 125200 g/mol (PDI = 2,44, GPC, PS standard), and the density was determined to be 1.051 g/cm^3 by means of an Helium Pycnometer. The used TiO_2 with size around 100 nm was procured from Riedel-de Haen 14027, Germany.

Preparation of Epoxy Blend

Blend of epoxy resin/ABS containing 3.6 wt % ABS were prepared using the melt mixing technique. ABS was first dissolved in epoxy resin at 180°C with constant stirring. After proper mixing, stoichiometric amount of DDS with an epoxy: amine ratio of 2: 1 was added as the curing agent and mixed well without changing the temperature. The resulting solution was poured in to an open mould. The blend was cured at 180°C for 3 h and then post cured at 200°C for 2 h in an air oven. After curing, blends were allowed to cool slowly to room temperature. Blends with ABS content 5 g in the epoxy-hardener mixture (100 g DGEBA + 35 g DDS) were prepared, and the samples were named as epoxy blend.

Preparation of Hybrid Composites

TiO_2 nanoparticles were dispersed in DGEBA (Epoxy)/ABS mixture and mixed at 180°C using a high speed magnetic stirrer for 2 h, amount of DDS with an epoxy: amine ratio of 2: 1 was added as the curing agent and mixed well. After proper mixing, composites were cured in an open mould at 180°C for 3 h and then post cured at 200°C for 2 h. Composites with TiO_2 content 0.4, 1, 5, and 10 g in the epoxy-hardener mixture (100 g DGEBA + 35 g DDS) were prepared, and the samples were named as 0.3 wt % TiO_2, 0.7 wt % TiO_2, 3.4 wt % TiO_2, and 6.7 wt % TiO_2.

Characterization

Scanning Electron Microscopy. Each sample was cooled and fractured in liquid nitrogen. After that the samples were sputtered with gold in the SCD 050 sputter coater to avoiding the charging effect. Finally, the sputtered samples were analyzed by using a Hitachi S-4800 high-resolution scanning electron microscope (SEM).

Transmission Electron Microscopy. Because of the lower penetration power of electrons, it is necessary to mount objects for examination in the electron microscope as very thin films. Therefore, samples were cut by using an ultramicrotom (ULTRACUT E. from REICHERT-JUNG) into 50 to 80 nm thick ultra thin films. After treating in the vapour of OsO_4, the stained samples were examined in the EM 902 transmission electron microscope (TEM) (Zeiss, Germany) with an accelerating voltage of 80 KV.

Thermogravimetric Analysis. Thermal stability of the hybrid composites was analyzed by thermogravimetric analysis (TGA). TA instrument Mettler Toledo TGA/SDTA/851 was used to monitor the samples. The measurements were performed on 3–5 mg of the samples from room temperature (25°C) to 700°C at a heating rate of 20°C/m and under nitrogen atmosphere.

Dynamic Mechanical Analysis. The investigation of the thermomechanical properties was performed using dynamic mechanical thermal analysis (DMTA) (DMA 2980, TA instruments). Rectangular specimens of 40 × 10 × 3 mm^3 were used. The analysis was done in single cantilever mode at a frequency of 1 Hz, from -100 to 300°C and at a heating rate of 1°C/min.

Tensile Properties. Specimens for mechanical testing were machined to the require dimensions from the cast laminates using cutting with a cutting machine. Tensile measurements were performed according to ASTM D 638. The measurements were taken with a universal testing machine (UTM) (Tinius olsen) Model H 50 KU at a cross-head speed of 10 mm/min. Rectangular specimens of 100 × 10 × 3 mm^3 were used for determining the tensile strength. The tests were performed on six different specimens of the same sample and the average was taken as the final value.

Impact Strength. Charpy impact strength of the hybrid composites was measured by means of a charpy Impact test following the specifications ISO 179/1eA. Impact tests were performed on Zorn Stendal impact testing machine. The dimensions of the specimens were approximately 40 × 8 × 4 mm^3.

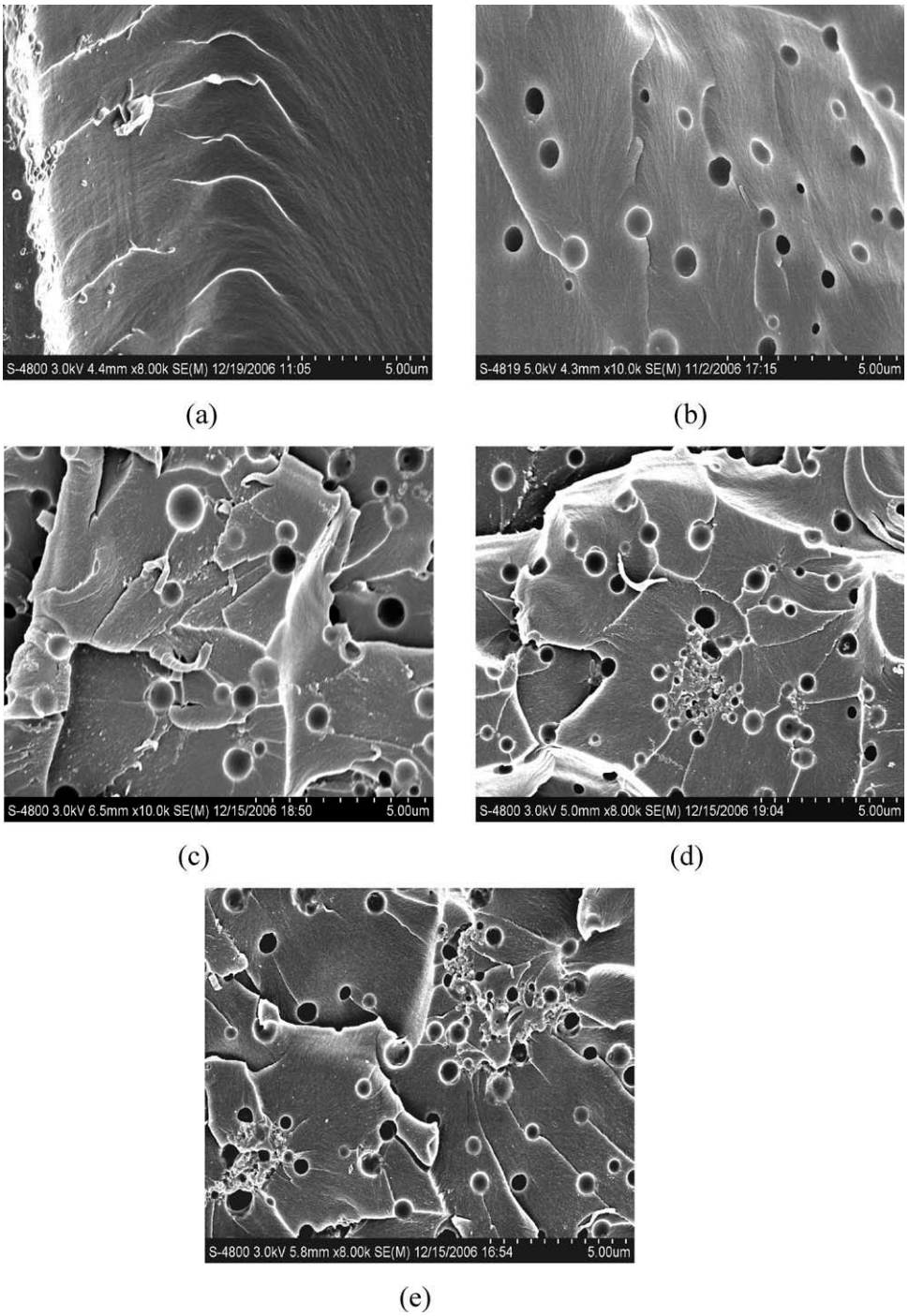

Figure 1. SEM micrographs of (a) neat epoxy, (b) blend, (c) 0.7 wt % TiO_2 hybrid composites, (d) 3.4 wt % TiO_2 hybrid composites, and (e) 6.7 wt % TiO_2 hybrid composites.

Fracture Toughness. Fracture toughness of the specimens was determined according to ASTM D 5045-99. The measurements were taken with a UTM Zwick (UPM-Z010). Rectangular specimens of 60 × 10 × 4 mm^3 were used for fracture toughness measurements. A notch of 5 mm was made at one edge of the specimen. A natural crack was made by pressing a fresh razor blade into the notch. The analysis was done in tension mode at room temperature. The value of stress intensity factor (K_{Ic}) was calculated using eq. (1).

$$\text{Stress intensity factor, } K_{Ic} = \frac{QPa^{1/2}}{bd} \quad (1)$$

where P is the load at the initiation of crack; a is the crack length; b is the breadth of the specimen; d is the thickness of

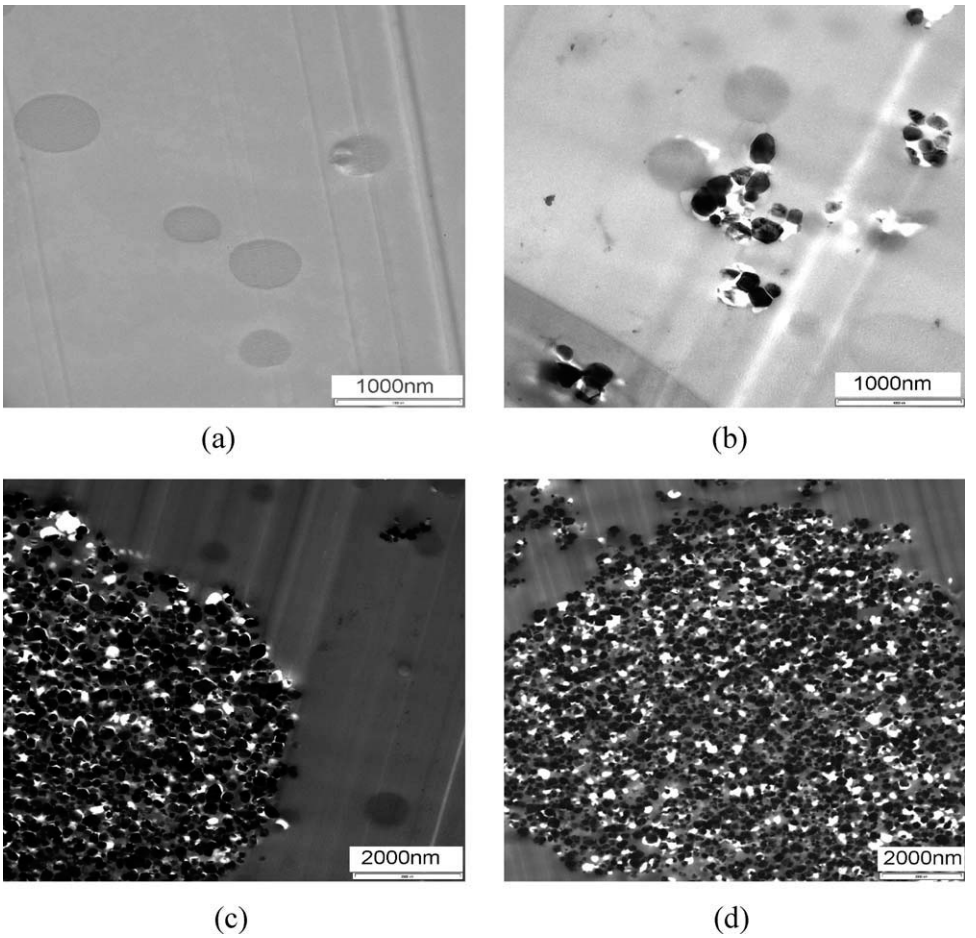

Figure 2. TEM micrographs of (a) blend, (b) 0.7 wt % TiO_2 hybrid composites, (c) 3.4 wt % TiO_2 hybrid composites, and (d) 6.7 wt % TiO_2 hybrid composites.

the specimen; and Q is geometry constant. Q is calculated using the following equation,

$$Q = 1.99 - 0.41(a/b) + 18.7(a/b)^2 - 38.48(a/b)^3 + 53.85(a/b)^4 \quad (2)$$

Field Emission SEM. The morphology of the fractured surface of cross-linked epoxy nanocomposites were examined using a ULTRA FESEM, (model-ultra plus) NanoTechnology Systems Division Carl Zeiss SMT AG, Germany. The fractured samples were coated with platinum by vapour deposition using a vacuum sputter.

RESULTS AND DISCUSSION

Electron Micrographs of Hybrid Composites

The surface morphology of the neat epoxy, blend, and hybrid composites was investigated by SEM. The SEM micrographs of cryogenically fractured surfaces of neat epoxy, DGEBA/ABS blend, and DGEBA/ABS/TiO_2 hybrid composites are shown in Figure 1. Figure 1(a) reveals the SEM micrograph of neat epoxy, which shows a flat homogeneous surface. For 3.6 wt % ABS-modified blend [Figure 1(b)], we have two phases, and the discrete thermoplastics with size around 400 nm were uniformly dispersed in the continuous epoxy matrix. Figure 1(c-e) shows the SEM micrographs of TiO_2 reinforced blend hybrid composites. In the basic matrix

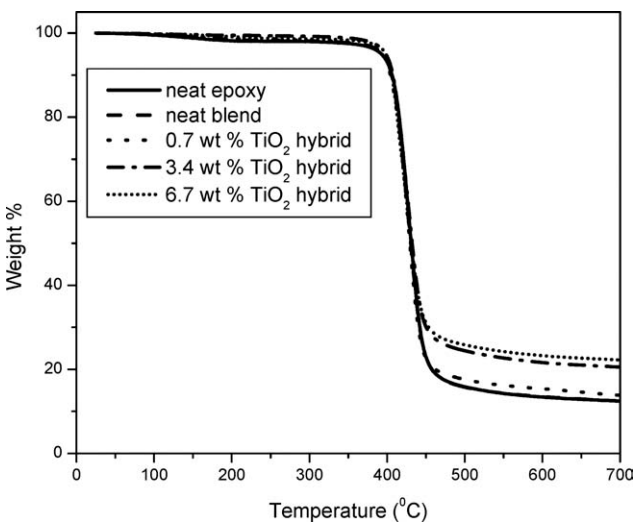

Figure 3. TGA curves for neat epoxy, blend, and hybrid composites.

Table I. % Char Content of Epoxy Hybrid Nanocomposites at Different Temperatures

	% Char content				
Temperature (°C)	Neat epoxy	Neat blend	0.7 wt % hybrid	3.4 wt % hybrid	6.7 wt % hybrid
100	99,51696	99,64303	99,60383	99,8241	99,8255
200	98,18266	98,50566	98,64375	99,483	99,1492
400	93,07576	93,20343	92,4995	94,4589	94,05729
500	15,85988	15,7487	17,58635	24,4298	25,84445
698	12,46874	12,49379	13,86243	20,5696	22,2806

droplet morphology, nanoparticles with size around 100 nm are attached to the epoxy matrix. From the micrographs, it can be seen that roughness of the surface increases with TiO_2 content.

The TEM micrographs of DGEBA/ABS blend and DGEBA/ABS/TiO_2 hybrid composites are shown in Figure 2. The effective utilization of TiO_2 in composite applications strongly depends on the ability to disperse them homogeneously throughout the matrix. To analyze the state of the dispersion of the filler in the polymer matrix, TEM micrographs were taken for the nanocomposites. For neat blend [Figure 2(a)], a heterogeneous surface with two phases are observed. For hybrid composites [Figure 2(b-d)], the particles are seems to be agglomerated and are dispersed in the epoxy/ABS blend matrix. The level of agglomeration increases with filler content. Because of the small size of the particles, the particle may hold together by weak van der waals force of attraction. Hence particles agglomerate in lumps; big lumps of nanoparticles were observed for 3.4 and 6.7 wt % TiO_2/ABS/epoxy nanocomposites [Figure 2(c,d)].

TGA

Thermal stability of neat epoxy, blend, and hybrid nanocomposites was studied by TGA and is shown in Figure 3. The weight percentage of the nanocomposites at different temperatures was taken and is given in Table I. From the Table, the average weight loss of around 1–2% up to 300°C is due to the release of moisture. The lack of weight loss at a temperature lower than 300°C indicates that there is no release of any molecules from the host during heating. However, the weight loss above 350°C is related to the decomposition of the polymer. From the Table, it can be seen that the thermal stability of the neat blend was not affected by the addition of TiO_2; however, after degradation at 700°C, the mass retained increased from 12 to 23 wt % for the polymer composites with increase in filler content. It is important to add that the char yield does not reflect the thermal stability, the increased char yield of the composites maybe results from the high char yield of TiO_2 rather than the resin.

DMA

DMA is a reliable technique to provide mechanical information because it involves the measurement of materials ability to store and dissipate mechanical energy when subjected to deformation under a wide range of temperature. The storage modulus demonstrates the load bearing capacity and the stiffness. Figure 4(a) shows the log E' curves of epoxy hybrid composites. From the profile, the storage modulus curves of epoxy hybrid composites are higher or comparable with 3.6 wt % ABS blend. The rigid TiO_2 particles improved the stiffness of the epoxy blend matrix composites and hence the load bearing capacity of the polymer composites. Their is an inflection

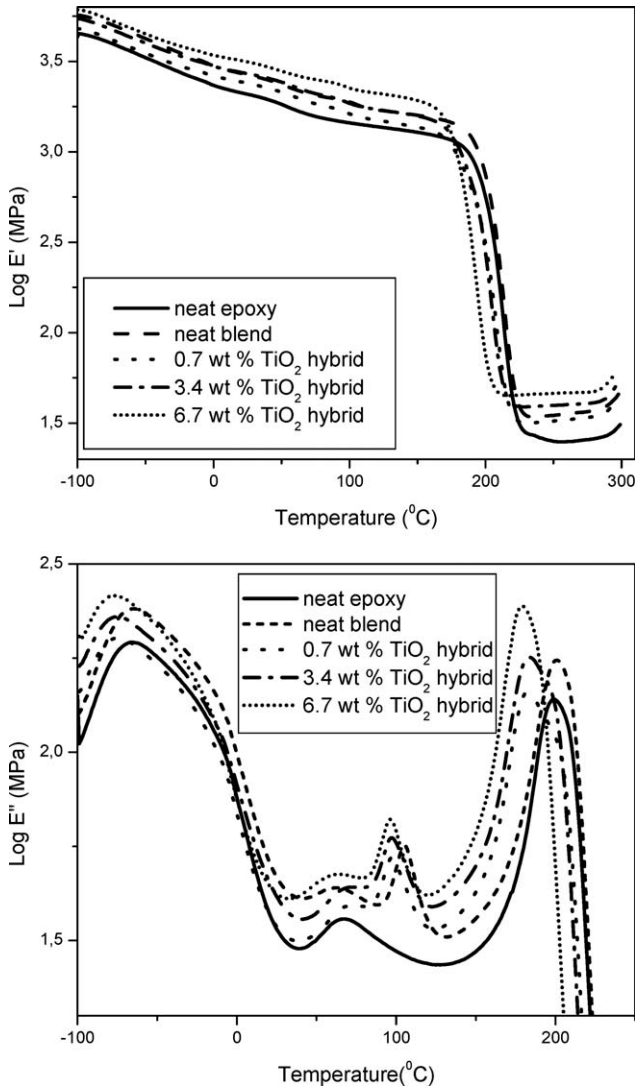

Figure 4. (a) Storage modulus curves for neat epoxy, blend, and hybrid composites. (b). Loss modulus curves for neat epoxy, blend, and hybrid composites.

Table II. T_g, M_c, and v_e of Different Epoxy Hybrid Nanocomposites

Sample	T_g (°C)	M_c (g/mol)	$\nu_e \times 10^{27}$ (chains/m^3)
Neat epoxy	200	358	2.02
Neat blend	200	358	2.02
0.7 wt % hybrid	182	428	1.69
3.4 wt % hybrid	182	428	1.69
6.7 wt % hybrid	179	438	1.65

point at around 200°C, which indicates the transition from solid state to the rubbery state: that means, the glass transition (T_g) of the system. The T_g of the cross-linked epoxy phase decreased by the addition of TiO_2, this is an indirect measure of cross-link density (Table II). This observable fact may be explained by postulating that the presence of TiO_2–epoxy interactions may reduce the cross-linking degree attained by the polymer matrix by preventing the complete curing of the epoxy (proved by non-isothermal DSC measurements, not shown here). After the T_g modulus decreases due the segmental mobility of the polymer chains.

The molecular weight between the cross-links (molecular weight of branches that make cross-links) (M_c), which is an indirect measure of cross-link density of epoxy resin, can be calculated from the T_g of the epoxy rich phase (DMA profile) using the following equation.[34]

$$M_c = \frac{3.9 \times 10^4}{T_g - T_{g0}} \tag{3}$$

where T_g is the glass transition temperature of the cross-linked epoxy resin and T_{g0} is the glass transition temperature of uncross-linked polymer having same composition as the cross-linked polymer. The value of T_{g0} was taken as 91°C for DGEBA/DDS system.[35] The effective cross-link density (v_e) was calculated from M_c using the following equation.[34]

$$\upsilon_e = \frac{\rho N_A}{M_c} \tag{4}$$

ρ is the density, and N_A is Avogadro's number.

The glass transition temperature, molecular weight between the cross-links (M_c) and the effective cross-link density (v_e) are summarized in Table II. The increase in M_c and consequent decrease in cross-link density with respect to the decrease in T_g was evident from the Table.

Log loss modulus (log E'') is a measure of the viscous response of the material. The log E'' recorded as a function of temperature for neat epoxy, blend, and hybrid composites and are shown in Figure 4(b). The neat epoxy resin shows only one transition region corresponding to the T_g of the cross-linked epoxy phase. However, blend and hybrid composites show two transitions corresponding to ABS and epoxy rich phase. The peak at lower temperature is due to thermoplastic phase and that at higher temperature is due to the epoxy rich phase. There is a shift in the epoxy glass transition toward the lower temperatures on increasing the nanofiller content because of lower cross-linking degree attained by the polymer matrix by the addition of TiO_2 particles. The loss moduli of the composites were increased on increasing the TiO_2 content because the dispersed TiO_2 dissipate energy due to resistance against viscoelastic deformation of the surrounding epoxy matrix.

Tensile Properties

Tensile properties of epoxy/ABS blend and hybrid composites are given in Table III. The data revealed a remarkable increment in tensile properties for 0.7 wt % TiO_2-modified hybrid nanocomposites. Because of the large surface area of nanomaterials, opportunities will be more for physical or chemical bonding with epoxy resin, thereby enhance the interfacial bonding of particles and substrate which would lead to improved properties of the nanocomposite. However, if the concentration of TiO_2 exceeds 0.7 wt %, the tensile toughness decreases. This suggests that the mechanical properties truly reflect on TiO_2 content and the state of dispersion of nanoparticles in the epoxy matrix. The increase in filler content makes it more difficult for dispersion and easier for nanosized particle to "agglomeration." Because agglomerated particles make it possible to generate defects on the material surface, stress concentration will likely occur within the epoxy due to external force, resulting in decreased tensile properties.[19] The tensile stress/strain curves of the blend systems given in Figure 5, reveals that tensile strain is also higher for 0.7 wt % TiO_2 nanocomposites than cured neat epoxy blend. The tensile toughness obtained from the area under the stress/strain curve shows an increment of twofold with 0.7 wt % TiO_2

Table III. Tensile Properties of Different Epoxy Hybrid Composites

Sample	Tensile strength (Mpa)	Tensile modulus (Gpa)	Tensile elongation (%)	Toughness (area under the stress/strain curves)
Neat epoxy	51 ± 4	2.3 ± 0.11	3.99 ± 0.2	121
Neat blend	65 ± 3	2.3 ± 0.12	6.93 ± 0.34	279
0.3 wt % hybrid	70 ± 3	2.3 ± 0.12	6.53 ± 0.28	288
0.7 wt % hybrid	80 ± 3	2.7 ± 0.12	8.49 ± 0.28	434
3.4 wt % hybrid	46 ± 2	2.7 ± 0.11	3.49 ± 0.16	95
6.7 wt % hybrid	43 ± 2	2.6 ± 0.12	2.91 ± 0.16	74

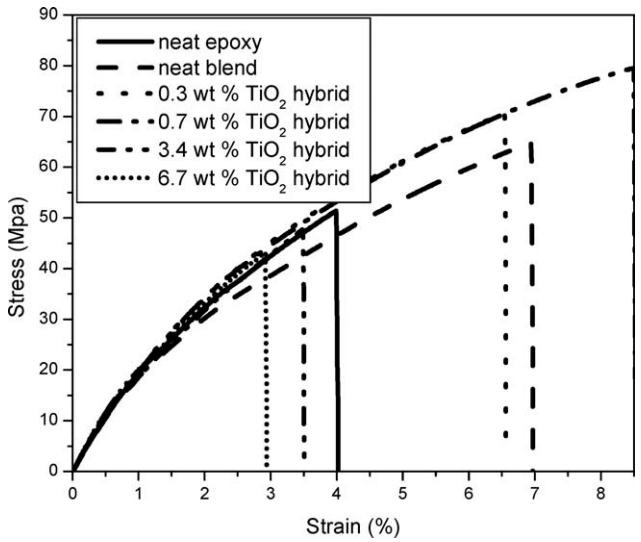

Figure 5. Tensile stress–strain curves of neat epoxy, blend, and hybrid composites.

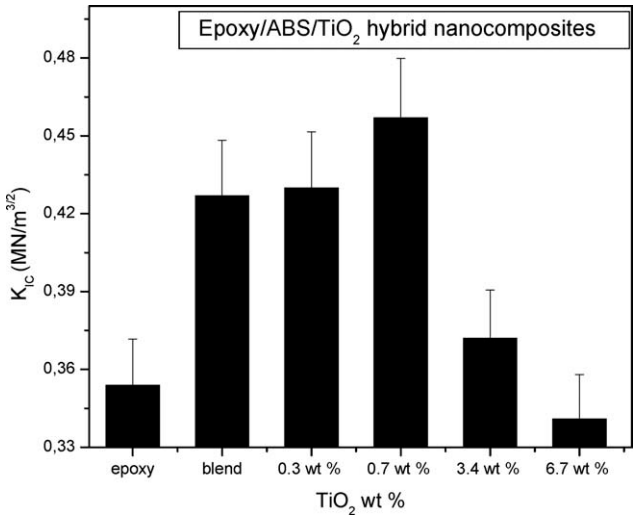

Figure 7. Fracture toughness of neat epoxy, blend, and hybrid composites (critical stress intensity factor).

nanocomposites with respect to the neat blend and fourfold with respect to neat cross-linked epoxy system.

Impact Properties

Impact strength of a material describes the energy required to break the specimen. The magnitude of the impact strength reflects the ability of the material to resist impact. Impact strength of cross-linked epoxy and epoxy composites were shown in Figure 6. Addition of 0.7 wt % TiO_2 particles increases the impact strength of the blend matrix slightly followed by a decrease. The decline in the impact strength can be attributed to the decreased toughness of the matrix. The above observation points toward agglomeration, and the nanosized particle tend to "agglomerate". Because agglomerated particles makes it possible to generate defects on the material surface, stress concentration will likely occur within the epoxy as a result of external force, resulting in a decreased impact strength.[16]

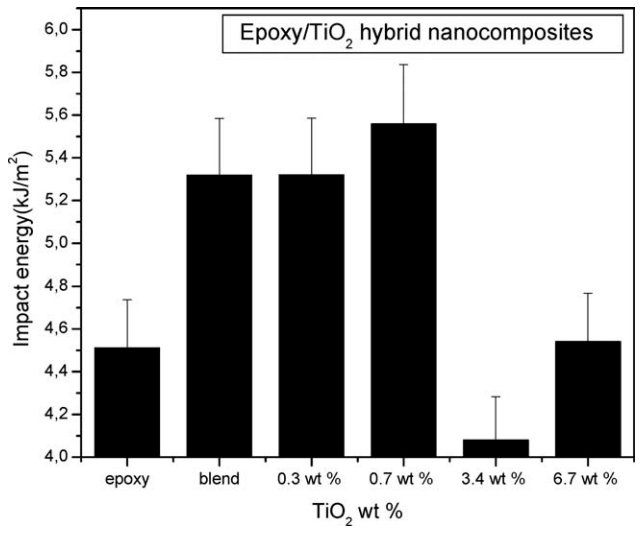

Figure 6. Impact energy (strength) of neat epoxy, blend, and hybrid composites.

Fracture Toughness

The resistance of a material to crack initiation and propagation can be explained in terms of fracture toughness. The fracture toughness of DDS-cured epoxy resin, 3.6 wt % ABS blend and hybrid composites was expressed as K_{Ic}. The variation of fracture toughness with composition is given in Figure 7. It can be seen that fracture toughness increased with the addition of TiO_2 to the blend matrix. The maximum fracture toughness is for 0.7 wt % TiO_2 hybrid composites; however, for higher filler content, the fracture toughness decreases because of the poor filler matrix interaction, the particles are unable to carry any part of the external load. In that case, the strength of the composite cannot be higher than that of the neat polymer matrix. Another important factor to be considered is related to the dispersion state of the nanoparticles, which may additionally play a significant role. For that case, relatively large agglomerates would remain in the matrix; a propagation crack could encounter a stress concentration locally and easily induce the initiation of the final failure.

Fracture Morphology

FESEM analysis of the fracture surface after fracture mechanics of TiO_2-filled cross-linked hybrid epoxy network gives an insight on the cause and location of failure as well as the dispersion state of the particles within the epoxy matrix. Figure 8 reveals the FESEM micrographs of samples observed under microscope after the K_{Ic} fracture test. The surface of unmodified cross-linked epoxy [Figure 8(a)] was smooth with free and regular crack propagation, indicating rather brittle fracture. From our previous studies, we have maximum toughness for 3.6 wt % ABS-modified epoxy blend because of the highly uniform dispersion of thermoplastic particles and also because of good interfacial adhesion.[12] The SEM of fractured surface of the 3.6 wt % ABS-modified

Applied Polymer SCIENCE

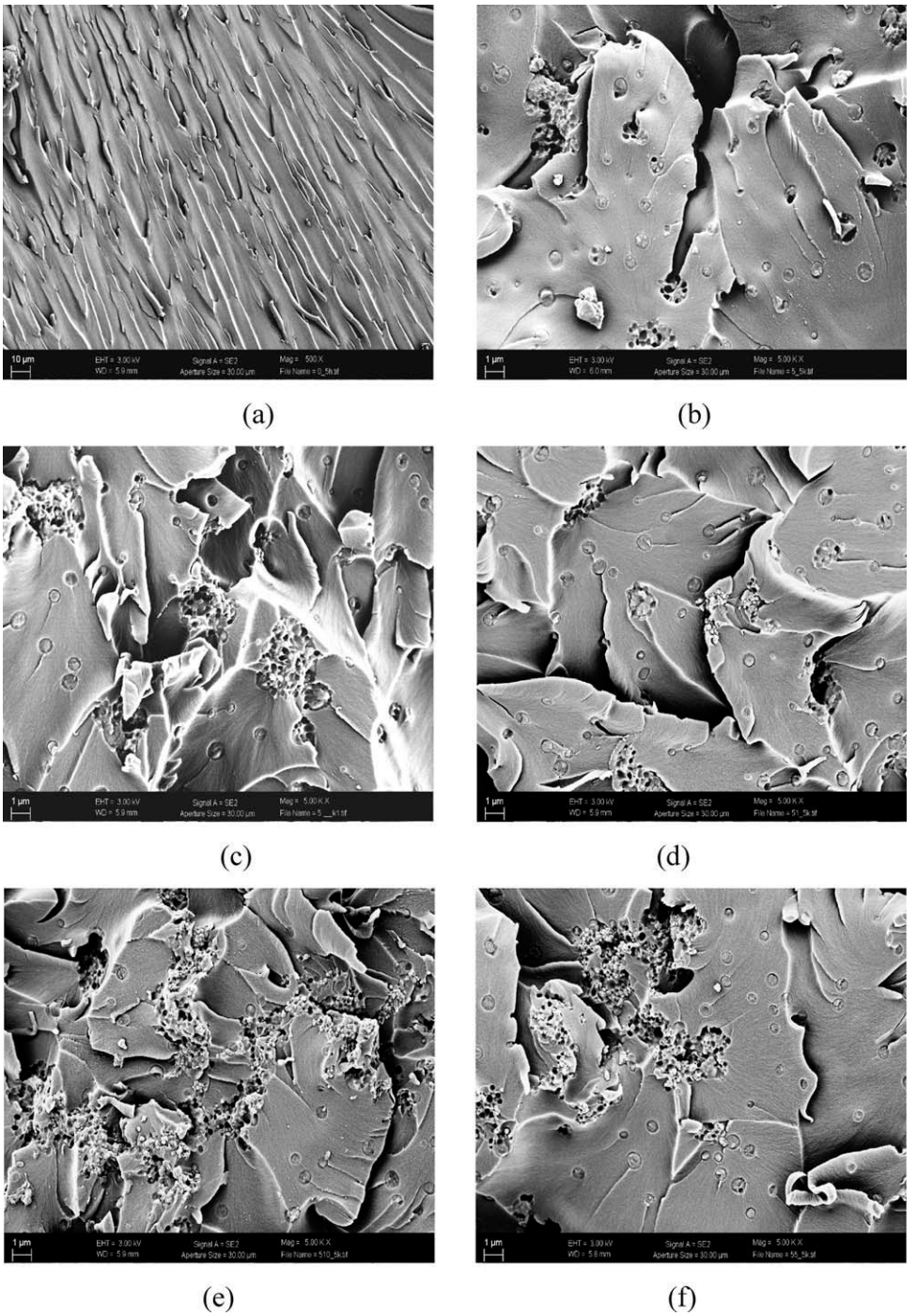

Figure 8. FESEM micrograph (fractured surface) of neat epoxy, blend, and hybrid composites (a) neat epoxy, (b) blend, (c) 0.3 wt % TiO_2 hybrid composites, (d) 0.7 wt % TiO_2 hybrid composites, (e) 3.4 wt % TiO_2 hybrid composites, and (f) 6.7 wt % TiO_2 hybrid composites.

epoxy blend, given in Figure 8(b), revealed the two-phase morphology, which is very important for toughness. Figure 8(c) reveals the fracture micrographs of 0.3 wt % TiO_2 hybrid composites, with few TiO_2 particles dispersed in the matrix.

From the fracture surface of 0.7 wt % TiO_2 hybrid composites [Figure 8(d)], the crack seems to be effected by the ABS droplets. The surface of the nanocomposite reveals some minor agglomerates, but between these agglomerates, the particles are separated well and distributed homogeneously within the polymer matrix, leading to a rough surface acting as obstacles for the propagating crack; subsequently, crack deflection occurs.[25] This fact leads to a higher fracture surface, which correlates with higher energy absorption during fracture. The synergic effect may be due the combined toughening effect initiated by both ABS and TiO_2 particles. It is important to mention that

the pioneer work by Pearson and coworkers[25,28] have established the cavitation effect in hybrid composites containing rubber. Accordingly, the presence of TiO_2 may enhance the rubber cavitation process. The stress whitening due to rubber particle cavitation and matrix dilation, is essential to the energy absorbing mechanism, and hence elevates the fracture toughness. The rubber particle cavitation releases tri-axial stress and may suppresses the debonding between TiO_2 and matrix. The suppressed debonding magnifies the crack pinning mechanism and further enhances the fracture toughness of the hybrid composites.[25] The roughness in surface shows that the systems become more ductile. With increase in filler loading above 0.7 wt %, the number of particles increases, that causes particle–particle interaction rather than particle–matrix interaction. Hence the particles begin to agglomerate and form lumps which eventually affect the van der waals interaction between the polymer chains and that may cause decrease in properties. The agglomerates of TiO_2 are believed to cause higher stresses in the polymer matrix near the particle edges, which will facilitate failure under fracture measurements. In the case of 3.4 wt % TiO_2 [Figure 8(e)], a morphology similar to 0.7 wt % TiO_2 was observed. But TiO_2 particles are more agglomerated. The fillers may act as failure sites. The particle clusters remaining in the matrix should be high enough for inducing a brittle and detrimental failure or in other words, TiO_2 particle clusters are high enough to inducing a brittle and detrimental failure in the way "large" particles would do and hence decline in properties. Similar observation was observed for 6.7 wt % TiO_2-modified blend system [Figure 8(f)].

CONCLUSION

The effect of TiO_2 loading on the ABS-modified epoxy resin composites were studied in detail. The results presented here showed that DDS-cured DGEBA/ABS blends were heterogeneous with a two-phase structure. The fracture toughness was increased substantially on blending and the increase in fracture toughness depends on the different factors such as composition, molecular weight, and curing parameters. The increase in fracture toughness can be explained using different mechanisms such as plastic deformation of the matrix, crack pinning, crack path deflection, and ductile tearing of the thermoplastic. However, for hybrid composites, the storage modulus increased with increase in filler loading and this was due to the reinforcement imparted by the stiff TiO_2 particles. We have very good improvement in mechanical properties as observed for 0.7 wt % TiO_2-modified ABS-epoxy system because of the synergetic effect imparted by both ABS and TiO_2 particles. However, at higher filler loading, the mechanical properties are lower than the base blend material due the particle agglomeration in hybrid composites. Because the particle size is too small, the tendency to agglomerate by van der waals force of attraction is more. The particle clusters remaining in the matrix should be high enough for inducing a brittle and detrimental failure.

REFERENCES

1. Fink, J. K. Epoxy Resins, Reactive polymers Fundamentals, and Applications, William Andrew: Norwich, NY, **2005,** p 240.
2. Kinloch, A. J. Adhesion and Adhesive Science and Technology; Chapman Hall: London, **1987.**
3. Bucknall, C. B.; Partridge, I. K. *Br. Polym. J.* **1983,** *15*, 71.
4. Bucknall, C. B.; Partridge, I. K. *Polymer* **1983,** *24*, 639.
5. Bennett, G. S.; Farris, R. J.; Thompson, S. A. *Polymer* **1991,** *32*, 1633.
6. Girard-Reydet, E.; Vicard, V.; Pascault, J. P.; Sautereau, H. *J. Appl. Polym. Sci.* **1997,** *65*, 2433.
7. Zheng, S.; Wang, J.; Guo, Q.; Wei, J.; Li, J. *Polymer* **1996,** *37*, 4667.
8. Di Pasquale, G.; Motta, O.; Recca, A.; Carter, J. T.; McGrail, P. T.; Acierno, D. *Polymer* **1997,** *38*, 4345.
9. Francis, B.; Ramaswamy, R.; Rao, V. L.; Jose, S.; Thomas, S.; Raju, K. V. S. N. *Polym. Eng. Sci.* **2005,** *45*, 1645.
10. Carter, J. T.; Emmerson, G. T.; Faro, C. L.; McGrail, P. T.; Moore, D. R. *Compos. Part A Appl. Sci. Manuf.* **2003,** *80*, 83.
11. Almen, G.; Byrens, R. M.; Mackenzie, P. D.; Maskell, R. K.; McGrail, P. T.; Sefton, M. S. *34th International SAMPE Symposium, Society for the Advancement of Material and Process Engineering,* California, USA, **1989,** *34*, 259.
12. Jyotishkumar, P.; Pionteck, J.; Häßler, R.; George, S. M.; Cvelbar, U.; Thomas, S. *Ind. Eng. Chem. Res.* **2011,** *50*, 4432.
13. Wetzel, B.; Rosso, P.; Haupert, F.; Friedrich, K. *Eng. Fract. Mech.* **2006,** *73*, 2375.
14. Chatterjee, A.; Islam, M. S. *Mater. Sci. Eng. A* **2008,** *487*, 574.
15. Zhao, R.; Luo, W. *Mater. Sci. Eng. A* **2008,** *483*, 313.
16. Huang, K. S.; Nien, Y. H.; Chen, J. S.; Shieh, T. R.; Chen, J. W. *Polym. Compos.* **2006,** *27*, 195.
17. Sarathi, R.; Sahu, R. K.; Rajeshkumar, P. *Mater. Sci. Eng. A* **2007,** *445*, 567.
18. Wetzel, B.; Haupert, F.; Zhang, M. Q. *Compos. Sci. Technol.* **2003,** *63*, 2055.
19. Al-Turaif, H. A. *Progr. Org. Coating* **2010,** *69*, 241.
20. Xian, G.; Walter, R.; Haupert, F. *J. Appl. Polym. Sci.* **2006,** *102*, 2391.
21. Sangermano, M.; Malucelli, G.; Amerio, E.; Bongiovanni, R.; Priola, A.; Di Gianni, A.; Voit, B.; Rizza, G. *Macromol. Mater. Eng.* **2006,** *291*, 517.
22. Nussbaumer, R. J.; Caseri, W. R.; Smith, P.; Tervoort, T. *Macromol. Mater. Eng.* **2003,** *288*, 44.
23. Xiong, M.; Zhou, S.; You, B.; Gu, G.; Wu, L. *J. Polym. Sci. Part B Polym. Phys.* **2004,** *42*, 3682.
24. Tong, Y.; Li, Y.; Xie, F.; Ding, M. *Polym. Int.* **2000,** *49*, 1543.
25. Azimi, H. R.; Pearson, R. A.; Hertzberg, R. W. *J. Appl. Polym. Sci.* **1995,** *58*, 449.
26. Marouf, B. T.; Pearson, R. A.; Bagheri, R. *Mater. Sci. Eng. A* **2009,** *515*, 49.

27. Liu, W.; Hoa, S. V.; Pugh, M. *Polym. Eng. Sci.* **2004,** *44*, 1178.

28. Liang, Y. L.; Pearson, R. A. *Polymer* **2010,** *51*, 4880.

29. Jyotishkumar, P.; Pionteck, J.; Häussler, L.; Haßler, R.; Thomas, S. *J. Appl. Polym. Sci.* in press.

30. Asif, A.; Rao, V. L.; Ninan, K. N. *Mater. Sci. Eng. A* **2010,** *527*, 6184.

31. Jyotishkumar, P.; Pionteck, P.; Özdilek, C.; Moldenaers, P.; Thomas, S. *Soft Matter* **2011,** *7*, 7248.

32. Jyotishkumar, P.; Thomas, S. *J. Macromol. Sci. Part A: Pure Appl. Chem.* **2011,** *48*, 751.

33. Jyotishkumar, P.; Pionteck, J.; Haßler, R.; Adam, G.; Thomas, S. *J. Macromol. Sci. Part B: Phys.* in press; doi: 10.1080/00222348.2011.629853.

34. Nielsen, L. *J. Macromol. Sci. Rev. Macromol. Chem. Phys.* **1969,** *C3*, 69.

35. Bellenger, V.; Verdu, J.; Morel, E. *J. Polym. Sci. Part B: Polym. Phys.* **1987,** *B25*, 1219.